Numerical Simulation of the Heat Dissipation During the Fatigue Test

Mohammad Zaeimi, Rosa De Finis, Davide Palumbo, and Umberto Galietti

Abstract Fatigue is an irreversible process accompanied by the heat dissipation which is significant when the transition from anelastic to inelastic strains happens. In view of this, in the last years, the heat dissipation has been accepted as an appropriate damage indicator of the material.

The estimation of the heat dissipation can be obtained by detecting the surface thermal footprint of the specimen by using thermography-based techniques. However, the energy dissipation as heat is highly sensitive to the environmental and test conditions and the microstructure status. Therefore, the experimental measurement is always associated with some inaccuracies and only provides an estimation of the heat dissipated during fatigue.

This paper is mainly focused on the numerical modeling of the heat dissipation performed by COMSOL Multiphysics software in order to investigate the factors that can affect the estimation of the heat source by means of thermography. The obtained results have been compared with an analytical solution derived from the one-dimensional heat equation. This study can provide valuable insights about the shape of the heat sources produced during the cyclic loading and differences associated with thermographic measurements and actual values, which are the main goals of this work.

Keywords Heat dissipation · Fatigue test · Thermography technique · Finite element simulation

Introduction

The study of fatigue phenomena remains an open issue because of the difficulties in modeling the material behavior and represents a key feature in choosing the most appropriate material since most of the mechanical components are subjected to dynamic loadings during their life [1].

Fatigue damage is an ambiguous phenomenon that forms and propagates mostly on a microscopic scale. Only when the damage has reached a critical level, it becomes detectable. In effect, by imposing a cyclic loading (depending on the loading level), the formation of dislocations is prompted. The accumulation of dislocations leads to plastic deformation. In turn, the occurrence and accumulation of microcracks are involved in macrocracks [2, 3]. Finally, the propagation of macrocracks induces material failure [4].

More insights on the phenomenon have been provided by Mareau et al. [5]. In particular, Mareau discussed two mechanisms of heat dissipations that occur during a fatigue test: (i) for low-stress amplitudes, an anelastic mechanism where the strains are irreversible and recoverable (e.g., the motion of dislocations, the migration of atoms, dislocation relaxation phenomena, and so on) and (ii) for high-stress amplitudes, an inelastic mechanism where the strains are irreversible but unrecoverable (e.g., the viscoplastic slip of dislocations). The transition from these two is the main cause of the strong dissipation and consequently the failure.

M. Zaeimi (✉) · D. Palumbo · U. Galietti
Department of Mechanics, Mathematics and Management, Polytechnic University of Bari, Bari, Italy
e-mail: mohammad.zaeimi@poliba.it; davide.palumbo@poliba.it; umberto.galietti@poliba.it

R. De Finis
Department of Engineering for Innovation, University of Salento, Lecce, Italy
e-mail: rosa.definis@unisalento.it

C. Franck et al. (eds.), *Challenges in Mechanics of Biological Systems and Materials, Thermomechanics and Infrared Imaging, Time Dependent Materials and Residual Stress, Volume 2*, Conference Proceedings of the Society for Experimental Mechanics Series,
https://doi.org/10.1007/978-3-031-50470-9_12

Of course, what happens to microscopic level determines an energy dissipation and a sentinel of this energy can be the surface temperature detected during a fatigue test. In this way, the aim of the present work is to investigate the capability of detected surface temperature to represent the temperature of inner heat source related to the fatigue damage.

One of the ways to take advantage of experimental techniques, particularly thermography, is to use them to detect the signature of materials undergoing to fatigue processes. In literature, different methods relying on the assessment of thermal signature have been developed to study the various aspects of fatigue damage in a rapid and reliable way [2, 6–8].

The first thermography-based method was the one proposed by Risitano [8] where a rapid method to study fatigue behavior of materials by assessing the temperature at stabilization of the material [8, 9] was investigated. In recent years, other different thermal features were investigated [10–23].

Enke and Sandor [10] for the first time showed the possibility of using the heat dissipation in the assessment of the damage of material. However, the quantification of the intrinsic dissipation, as an appropriate index for fatigue characterization, is a big challenge due to the fact that it is significantly dependent on the accuracy of temperature acquisition process and simplifications applied on heat equation for deriving it; therefore, a certain deviation always exists for these estimations [24–30]. Besides the estimations based on the mean temperature [31, 32], two other effective ways to estimate the heat dissipation are both studying the second amplitude harmonic (SAH) of temperature [10, 21, 33, 34] and the plastic work (hysteresis loop) [22], as they are completely related to the plastic deformation which is the main cause of the dissipation. Enke and Sandor [9] found the SAH effect by imposing the Fourier sine series on the thermal signal and proposed that the amplitude at the frequency twice the frequency of the mechanical loading is proportional to the plastic strains or intrinsic dissipation [34, 35].

In this study, a numerical model was defined to compare the heat dissipation experimentally estimated by measuring surface temperature and the numerical one using a FEM model that simulates the heat source. The effect of the amplitude and size of the heat source on the simulated temperature is also studied. The difference between measured and simulated temperature and energy values are also showed for different case studies. The present study could represent a step forward in understanding the difference between energy dissipations from the real heat source and energy dissipations assessed via thermography. It should be noted that the experimental values are taken from work by De Finis et al. [21].

The paper is organized as follows. First, the numerical model is proposed, and its correctness is shown by comparing the results with an analytical solution. Next, it is proposed how a heat source can be estimated in terms of magnitude and shape; and finally, the conclusion and future works are presented.

Numerical Simulation of the Heat Source

One way to ensure about the accuracy of a numerical model, especially in the case of cyclic heat source, is searching for a model that can provide an analytical solution. Generally, for an isotropic and homogeneous material, the first law of thermodynamics applied to a control volume surrounding the gage section of a sample in terms of energy per second (power) gives:

$$\underbrace{\int \left(\rho C \frac{\partial T}{\partial t}\right) dV}_{\text{Internal energy}} = \left[\underbrace{\int \left(k \nabla^2 T\right)\, dV}_{\text{Conduction}} - \underbrace{\int h\,(T - T_\infty)\, dA}_{\text{Convection}} - \underbrace{\int \epsilon\beta \left(T^4 - T_\infty^4\right) dA}_{\text{Radiation}} \right] + \underbrace{\int (\sigma : d\varepsilon)\, f\, dV}_{\text{Mechanical energy}} \tag{1}$$

where ρ, C, T, and T_∞ are correspondingly the density, specific heat at constant pressure, and absolute and ambient temperatures; h, k, ϵ, and β are, respectively, the convection coefficient, thermal conductivity, emissivity, and Stephan-Boltzmann constant; A, V, σ, ε, and f are, respectively, the area, volume of the gauge section, the Cauchy stress tensor, strain tensor, and cyclic frequency. Assuming that the cross section of the specimen in the gage section is constant, the temperature distribution in one-dimensional model with a heat power $\dot{Q}$is [36]:

$$\frac{\partial^2 T}{\partial z^2} - \frac{hP}{Ak}(T - T_\infty) - \epsilon\beta \frac{P}{Ak}\left(T^4 - T_\infty^4\right) - \frac{\dot{Q}}{k} = \frac{1}{\alpha}\frac{\partial T}{\partial t} \tag{2}$$

where P is the perimeter of the cross section of the sample and α is the thermal diffusivity. Since T is the absolute temperature ($T - T_\infty \ll T_\infty$), it is feasible to linearize the third term by Taylor expansion around T_∞. Thus, Eq. (5) will be reduced to the following partial differential equation (PDE) [36]:

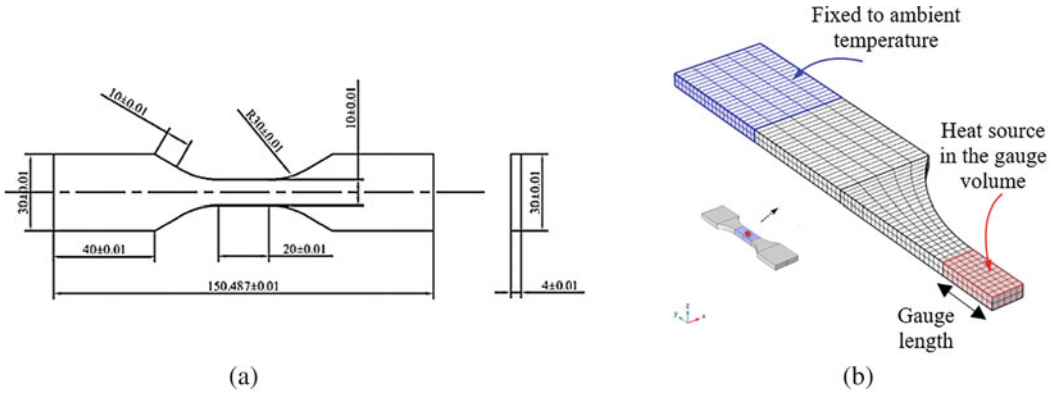

Fig. 1 (**a**) Sample geometry for comparison with an analytical approach [23] and (**b**) FEM modeling

$$\begin{cases} \frac{\partial^2\theta}{\partial z^2} - m^2\theta + \frac{\dot{Q}}{k} = \frac{1}{\alpha}\frac{\partial\theta}{\partial t} \\ \theta\,(0,t) = \theta\,(L,t) = 0 \quad ,\theta\,(z,0) = 0 \end{cases} \tag{3}$$

where $\theta = T - T_\infty$, $m = \sqrt{\frac{(h+4\epsilon\beta T_a^3)P}{Ak}}$ and L is the effective length. Maple programming language was utilized to solve Eq. (3) which is a linear non-homogenous partial differential heat equation. The solutions are as follows:

- For a constant heat, $\dot{Q} = H\ \left(\frac{W}{m^3}\right)$

$$\theta\,(z,t) = \frac{1}{km^2\left(e^{2mL}-1\right)}\left\{\left(e^{mz} - e^{m(L+z)} - e^{m(2L-z)} + e^{2mL} + e^{m(L-z)} - 1\right)H + \left(\sum_{n=1}^{\infty}\frac{2\,\sin\left(\frac{n\pi z}{L}\right)e^{-\frac{\alpha t\left(L^2m^2+\pi^2n^2\right)}{L^2}}HL^2\left((-1)^n-1\right)}{\pi nk\left(L^2m^2+\pi^2n^2\right)}\right)e^{(2mL-1)}m^2k\right\} \tag{4}$$

- For a cyclic heat, $\dot{Q} = H\,(1+\sin(2\pi f t))\ \left(\frac{W}{m^3}\right)$

$$\theta\,(z,t) = \sum_{n=1}^{\infty}\frac{1}{kn\pi\left(L^2m^2+\pi^2n^2\right)\left(\left(L^2m^2+\pi^2n^2\right)^2\alpha^2+\omega^2L^4\right)}\left\{2\left(-1+(-1)^n\right)\ HL^2\sin\left(\frac{n\pi z}{L}\right)\left(\left(\left(L^2m^2+\pi^2n^2\right)^2\alpha^2 - \omega L^2\left(L^2m^2+\pi^2n^2\right)\alpha+\omega^2L\right)e^{-\frac{\alpha t\left(L^2m^2+\pi^2n^2\right)}{L^2}} + \omega L^2\left(L^2m^2+\pi^2n^2\right)\alpha\cos(\omega t) - \left(L^2m^2+\pi^2n^2\right)\alpha^2\sin(\omega t) - \left(L^2m^2+\pi^2n^2\right)^2\alpha^2+\omega^2L^4\right)\right\} \tag{5}$$

where H is the mean value of each heat dissipated power. As shown in Fig. 1a, due to the symmetry of the dog bone sample, only 1/8 of the geometry was modeled with appropriate boundary conditions, shown in Fig. 1b. Hexahedral elements with quadratic Lagrange discretization are used for meshing, and after mesh convergence study, it was meshed with 1260 elements. The temperature at both ends (the domain in blue) was assumed to be fixed to the environmental temperature, T_∞.

For comparison, $H = 10^7(\mathrm{W/m^3})$, a thickness of 6 mm, and the C45 steel as the material with parameters listed in Table 1 (all taken from the study by De Finis et al. [23]) were considered. As shown in Fig. 2, the FEM and analytical results are comparable for both constant and cyclic heat source.

In the last second of the simulation, the mean temperatures from numerical and analytical results are 26.164 °C and 26.125 °C, respectively, which give only 0.15% error. In addition, in terms of the temperature amplitude, the error is

Table 1 Input parameters for comparison between the analytical and numerical results; for material C45 [23]

ρ (kg/m^3)	C_p(J/kg ° C)	k(W/m ° C)	α (1/ ° C)	h(W/m^{2}K)	T_∞(°C)	ϵ	f(Hz)
7850	486	42.5	13.3	5	20	0.98	11

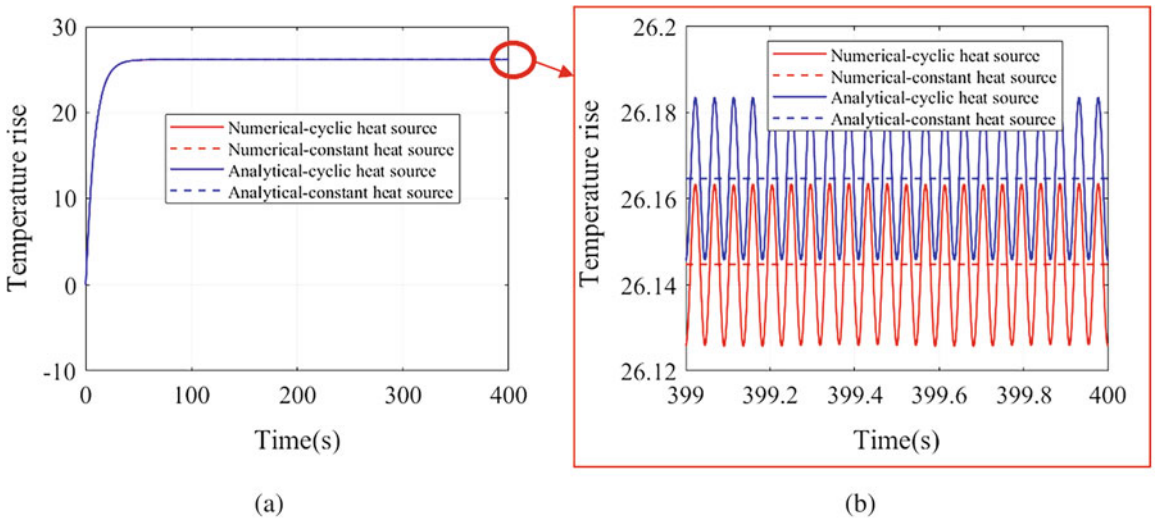

Fig. 2 (**a**) Numerical and analytical results comparison for constant heat source and (**b**) cyclic heat source

about 2.09% with the amplitudes of 0.0191 °C and 0.0195 °C related to the numerical simulation and analytical solution, correspondingly.

Heat Source Identification

In the previous section, the correctness of the numerical model was shown using an analytical 1D model. In this section, the heat source producing the temperature values in terms of second harmonic temperature variations is simulated considering also the effect of geometry. The aim is to investigate differences between the experimentally measured values of SAH and the same values determined from numerical model.

For this purpose, the experimental results were taken from a recent work by De Finis et al. [23] which focused specifically on the possibility of utilizing the SAH of temperature signal as an indicator to predict the heat dissipated energy. As mentioned by Krapez et al. [35], this temperature component completely related to the intrinsic dissipation especially in fully reversed loading. In recent years, researchers have shown their interests in this temperature component and recognized it as an effective index on the fatigue limit prediction [21–23, 33–35, 37].

In general, as mentioned by De Finis et al. [23], a cyclic load causes periodic behaviors for both strain and stress during the fatigue test. Consequently, according to the first law of thermodynamic, in terms of energy rates and ignoring the stored energy rate, the dissipated heat during a cyclic process (under fully reversed loading, $R = -1$) is almost equal to mechanical energy $\dot{E}_d \approx \dot{W}$; therefore, the heat dissipated energy rate, $\dot{E}_d$, is also a periodic function [23]. Imposing DFT (discrete Fourier transform), the second amplitude harmonic of $\dot{E}_d$, $\dot{E}_{d_a}^{2\omega}$, can be evaluated based on the SAH of temperature as the fundamental dissipative temperature component [23]:

$$\dot{E}_{d_a}^{2\omega} = 2f\rho C T_a^{2\omega} \tag{6}$$

where $2f$ shows twice the frequency of the loading and $T_a^{2\omega}$ is the second harmonic amplitude of the temperature associated to E_d and imposing DFT [23].

The experimental value of $\dot{E}_{d_a}^{2\omega}$ for the loading step with stress amplitude of 340 MPa and fully reversed loading condition is 9.59×10^5 (W/m^3) [23]; by using Eq. (6) and the measured value of SAH: $T_{a\,\mathrm{exp}}^{2\omega}$=0.0114 (°C). Of course, since $T_a^{2\omega}$ was from the surface temperature data, $\dot{E}_{d_a}^{2\omega}$ is only an estimation of its real value [23].

Table 2 Surface $T^{2\omega}_{a_{\text{num}}}$ for different heat source amplitude $\dot{E}^{2\omega}_{d_a}$ and $\dot{W}^{2\omega}_{a}$ and comparison with the corresponding experimental value

Heat source (W/m^3)		Gauge volume fraction				
		1/15	2/15	5/15	10/15	1
$d = \dot{E}^{2\omega}_{d_a}\ (1 + \sin(2\pi\ (2f)\ t))$	$T^{2\omega}_{a_{\text{num}}}$ (°C)	0.0002	0.0003	0.0007	0.0014	0.0018
	$T^{2\omega}_{a\,\text{exp}} / T^{2\omega}_{a_{\text{num}}}$	54.2857	33.5294	15.4054	8.2014	6.1957
$d = \dot{W}^{2\omega}_{a}\ (1 + \sin(2\pi\ (2f)\ t))$	$T^{2\omega}_{a_{\text{num}}}$ (°C)	0.0092	0.0137	0.0315	0.0597	0.0789
	$T^{2\omega}_{a\,\text{exp}} / T^{2\omega}_{a_{\text{num}}}$	1.2391	0.8321	0.3619	0.1910	0.1445

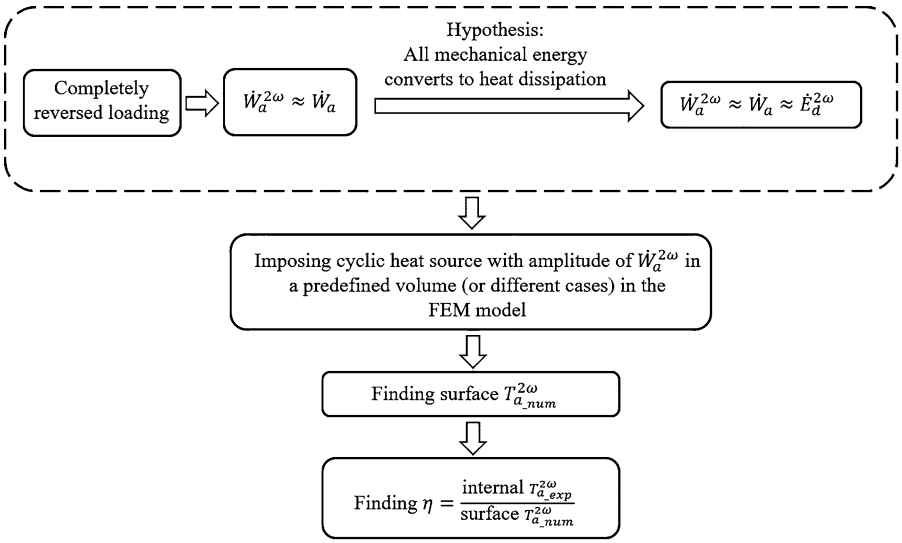

Fig. 3 A schematic representation of heat source identification

Using this value, the geometry, and mechanical properties proposed in Fig. 1 and Table 1, the simulations were performed for four fractions of the gauge volume (the gauge volume is shown in Fig. 1b) in addition to the whole gauge volume because the volume producing heat is unknown. It should be noted that smaller volumes are considered to be the same as the gauge volume, but they are shrunk only in y direction from both ends to provide each fraction. Similar to the experimental procedure in thermography-based technique, the temperature data obtained from the simulation are examined only from the surface of the gauge volume. The input parameters, mesh, and boundary conditions are the same as previous section, and the cyclic heat source was $d = \dot{E}^{2\omega}_{d_a}\ (1 + \sin(2\pi\ (2f)\ t))\ \left(W/m^3\right)$.

As shown in Table 2, comparing experimental $T^{2\omega}_{a}$ with the numerical one, reveals a big difference even considering the whole of the gauge length producing heat which is not prevalent in the fatigue test. This difference is associated to different causes; one of them can be related to the procedure of measuring the dissipated heat which is based on the acquisition of surface temperature.

Since the experimental value of $\dot{E}^{2\omega}_{d_a}$ was measured from the surface, it cannot be a representative of the real heat source at twice the frequency of the loading; thus it is worth utilizing a much more reliable experimental value: the SAH of the mechanical energy rate, $\dot{W}^{2\omega}_{a}$, that can be obtained from $\dot{W}$ (strains from extensometer and stresses from loading machine) after applying DFT [23].

It should be noted that in a fully reversed loading, the second harmonic component of the mechanical energy is almost equal to the total mechanical energy [19]. For $R = -1$ and the considered material, it can be also assumed that the mechanical energy is totally converted to heat, so under these conditions $\dot{W}^{2\omega}_{a}$ can be used as the parameter representing the total heat dissipation. For clarification, the procedure is schematically presented in Fig. 3.

By considering a cyclic heat source in the form of $d = \dot{W}^{2\omega}_{a}\ (1 + \sin(2\pi\ (2f)\ t))\ \left(\text{W/m}^3\right)$, as shown in Table 2 and $\dot{W}^{2\omega}_{a} = 4.11 \times 10^7\ \left(\text{W/m}^3\right)$ [23], the surface $T^{2\omega}_{a_{\text{num}}}$ approaches to $T^{2\omega}_{a}$ exp when the heat volume is between 1/15 and 2/15 of the gauge volume. This portion of volume seems to show that the plastic deformation occupied not the whole but a portion of the gauge volume as it can be expected in the fatigue failure. Thus, at this stage, the heat volume that can produce acceptable $T^{2\omega}_{a}$on the surface of the gauge volume is found, numerically. Of course, more investigations to explain physically this result are required.

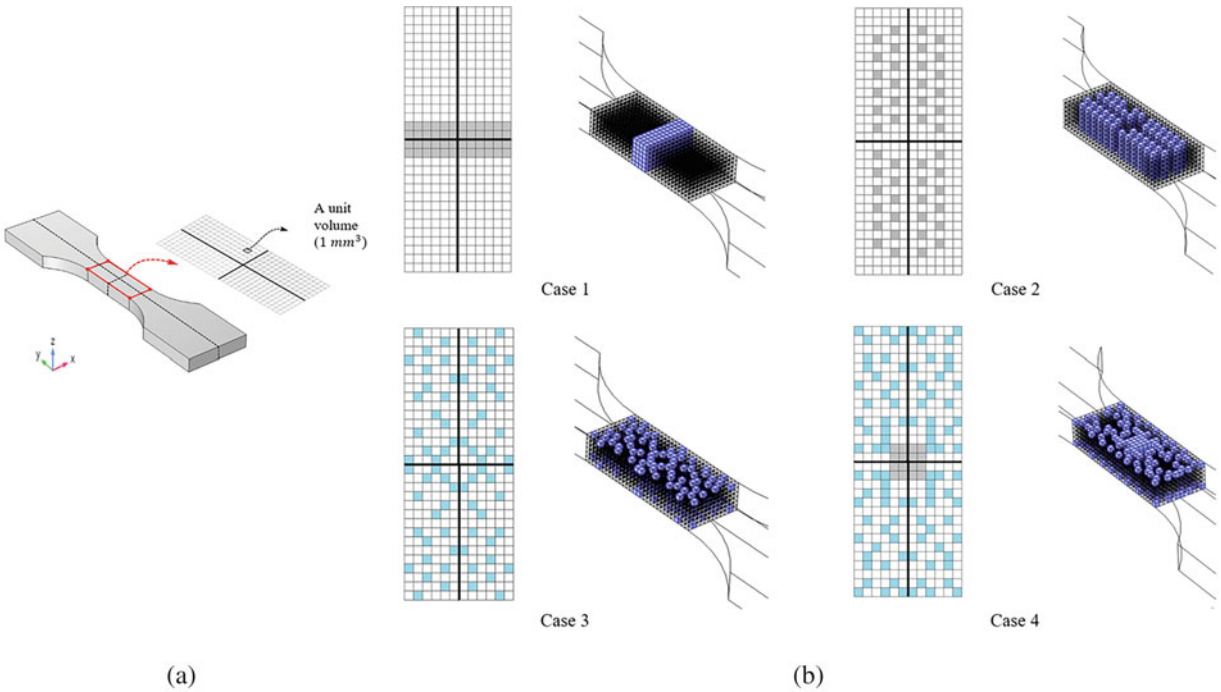

Fig. 4 (**a**) Grid on the surface of the gauge length; (**b**) representation of different heat source geometries

Table 3 Geometry of each volume(s) in each case

Case #	Number of separated volumes	Length (mm) of volume edge in		
		x-direction	y-direction	z-direction
1	1	12	4	6
2	48	1	1	6
3	144	1	1	2
4	1	4	4	6
	192	1	1	1

Furthermore, it is of great importance investigating the influence of the geometry of the heat volume on surface $T_a^{2\omega}$ since considering a single integrated volume, for example, 2/15 of the gauge volume as presented in Fig. 4b and Case 1, is almost impossible during the fatigue test, since there are lots of regions (i.e., the defects existing both inside and on the surface of the material) which can produce heat when deformed plastically.

For this purpose, as can be seen in Fig. 4b, the geometry of the heat source was changed for three more cases to check what happens to the temperature amplitude. A schematic representation is proposed to introduce different cases. As shown in Fig. 4a, the red border, the surface of the gauge volume, contains a set of squares (or elements) representing the top surface of a cube with the volume of 1 mm^3 where a heat source can be located. The thick black horizontal and vertical lines on the grid show the symmetric planes of the dog bone sample. The considered cases are presented with two colors, and each color shows how the heat source is spread through the thickness. The gray color is for a volume with boundary from the top to bottom of the gauge volume, while the blue color is related to volumes spread only on the top and bottom surfaces of the gauge volume. It should be noted that all cases are assumed to have a fixed volume of 2/15 gauge volume as this fraction provides acceptable surface $T_a^{2\omega}$ (please see Table 2). In addition, the geometry of the volume(s) in each case is listed with details in Table 3. In Case 4, a more real form of a heat volume was modeled. It is assumed that there are some small volumes on the surface (they can be a representative of the damage accumulation sites and possible crack triggers) with a relatively big one in the center of the gauge length (it shows damage accumulation which is highly possible to be presented with a fully reversed load).

From Table 4, the surface $T_{a_{\text{num}}}^{2\omega}$ is significantly affected by the heat source geometry in which it decreases by 10.95% for Case 2 and increases, respectively, by 37.96% and 106.57% for Case 3 and 4, if compared with Case 1.

Table 4 Numerical surface $T_a^{2\omega}$ with $d = \dot{W}_a^{2\omega}\ (1 + \sin(2\pi\ (2f)\ t))\ \left(W/m^3\right)$ for different heat volume geometries

	Surface $T_{a_{\text{num}}}^{2\omega}$	$\eta = \frac{\text{internal } T_{a\,\text{exp}}^{2\omega}}{\text{surface } T_{a_{\text{num}}}^{2\omega}}$
Case 1	0.0137	35.69
Case 2	0.0122 (-10.95%)	40.08
Case 3	0.0189 (+37.96%)	25.87
Case 4	0.0283 (+106.57%)	17.28

In addition, for the heat amplitude equal to $\dot{W}_a^{2\omega}$, a comparison between numerical surface $T_a^{2\omega}$ where temperature is measured and the related value inside the gauge volume, called internal$T_{a\,\text{exp}}^{2\omega}$, is presented. As assumed previously and shown in Fig. 3, with the total heat dissipation almost equal to $\dot{W}_a^{2\omega}$, the internal$T_{a\,\text{exp}}^{2\omega}$ can be calculated to be equal to 0.489 directly by replacing $\dot{W}_a^{2\omega}$ instead of $\dot{E}_{d_a}^{2\omega}$ in Eq. (6). For this purpose, the ratio of internal $T_{a\,\text{exp}}^{2\omega}$ to the surface$T_{a_{\text{num}}}^{2\omega}$ (η) is calculated and compared with the experimental one in the work by De Finis [23], which was almost equal to 20. Note that they found a linear relation between $\dot{W}_a^{2\omega}$ and $\dot{E}_{d_a}^{2\omega}$ [23] which is the same as the relation between $T_{a\,\text{exp}}^{2\omega}$ and $T_a^{2\omega}$ as the latter two can be obtained by dividing the related energy components by $2f\,\rho C_p$ (see Eq. (6)).

It can be seen from the last lines (Case studies 3 and 4) of Table 4 that η is relatively close to the above experimental ratio of 20. It shows the volume in the form of Case 4 can be a possible geometry for the real heat source in the fatigue test done by De Finis [23]. As a conclusion, more trial heat volume geometries can also be examined numerically and checked in the same way for the considered four cases to understand better the volumes producing heat, in future works.

Conclusion

In this work, a numerical model has been proposed to estimate the heat source in terms of the amplitude and geometry. It was compared with an analytical solution of a one-dimensional heat equation to be ensured if the model works precisely. Comparing with the analytical solutions for constant and cyclic heat sources, the errors were below 5% which is evident for the accuracy of the model. The results from modelling four possible heat volumes show that the SAH of temperature component, as the fundamental dissipative temperature component, is significantly dependent on both the size and shape of considered volumes.

In addition, comparing the ratio of the numerical and experimental SAHs of surface temperature to the experimental one inside the gauge volume is shown to provide an insight into the real heat volume identification.

This study can be regarded as preliminary work aimed to investigate the heat volumes created during the fatigue test and determine the relationship between the actual heat sources and the superficial temperatures obtained via thermographic measurements. Future works will investigate more heat volumes and will study other geometries of the samples and other thermal components.

References

1. Schijve, J.: Fatigue of Structures and Materials. Springer, Dordrecht (2009)
2. Bjørheim, F., Siriwardane, S.C., Pavlou, D.: A review of fatigue damage detection and measurement techniques. Int. J. Fatigue. **154**, 106556 (2022)
3. Subra, S.: Fatigue of Materials. Cambridge Solid State Science Series (1992)
4. Mughrabi, H.: Cyclic slip irreversibilities and the evolution of fatigued. Metall. Mater. Trans. A. **40**, 1257–1279 (2009)
5. Mareau, C., Favier, V., Weber, B., Galtier, A., Berveiller, M.: Micromechanical modeling of the interactions between the microstructure and the dissipative deformation mechanisms in steels under cyclic loading. Int. J. Plast. **32–33**, 106–120 (2012)
6. Vollmer, M., Möllmann, K.-P.: Infrared Thermal Imaging: Fundamentals, Research and Applications. Wiley (2011)
7. Maldague, X.: Theory and Practice of Infrared Technology for Nondestructive Testing. Wiley (2001)
8. Geraci, A., La Rosa, G., Risitano, A.: L'infrarosso termico nelle applicazioni meccaniche. ATA Ingegneria Automotoristica Catania, Italy (1983)
9. Luong, M.: Infrared thermographic scanning of fatigue in metals. Nucl. Eng. Des. **158**, 363–376 (1995)
10. Enke, N.F., Sandor, B.I.: Cyclic plasticity analysis by differential infrared thermography. In: Proceedings of the VII International Congress on Experimental Mechanics, pp. 830–835 (1988)
11. Kaleta, J., Blotny, R., Helmuth, H.H.: The accumulated internal energy in the fatigue strength region. In: Proceedings of the 7th International Conference on Fracture, pp. 1195–1202 (1989)
12. Luong, M.: Fatigue limit evaluation of metals using an infrared thermographic technique. Mech. Mater. **28**, 155–163 (1998)

13. Fargione, G., Geraci, A., Rosa, G.L., Risitano, A.: Rapid determination of the fatigue curve by the thermographic method. Int. J. Fatigue. **24**, 11–19 (2002)
14. Curà, F., Curti, G., Sesana, R.: A new iteration method for the thermographic determination of fatigue limit in steels. Int. J. Fatigue. **27**, 453–459 (2005)
15. Boulanger, T., Chrysochoos, A., Mabru, C., Galtier, A.: Calorimetric analysis of dissipative and thermoelastic effects associated with the fatigue behavior of steels. Int. J. Fatigue. **26**, 221–229 (2004)
16. Maquin, F., Pierron, F.: Heat dissipation measurements in low stress cyclic loading of metallic materials: from internal friction to microplasticity. Mech. Mater. **41**, 928–942 (2009)
17. Naderi, M., Khonsari, M.M.: An experimental approach to low-cycle fatigue damage based on thermodynamic entropy. Int. J. Solids Struct. **47**, 875–880 (2010)
18. Wang, X., Crupi, V., Jiang, C., Guglielmino, E.: Quantitative Thermographic Methodology for fatigue life assessment in a multiscale energy dissipation framework. Int. J. Fatigue. **81**, 249–256 (2015)
19. De Finis, R., Palumbo, D., Galietti, U.: A multianalysis thermography-based approach for fatigue and damage investigations of ASTM A182 F6NM steel at two stress ratios. Fatigue Fract. Eng. Mater. Struct. **42**, 267–283 (2019)
20. Lipski, A.: Change of specimen temperature during the monotonic tensile test and correlation between the yield strength and thermoelastoplastic limit stress on the example of aluminum alloys. Materials. **14**(1), 13 (2021)
21. De Finis, R., Palumbo, D., Pirinu, A., Saponaro, A., Panella, F.W., Nobile, R., Galietti, U.: Fatigue behaviour assessment of C45 steel by means of energy-based methods. IOP Conf. Ser. Mater. Sci. Eng. **1038** (2021)
22. Meneghetti, G., Ricotta, M.: Estimating the intrinsic dissipation using the second harmonic of the temperature signal in tension-compression fatigue, Part II: experiments. Fatigue Fract. Eng. Mater. Struct. **44**, 2153–2167 (2021)
23. De Finis, R., Palumbo, D., Galietti, U.: On the relationship between mechanical energy rate and heat dissipated rate during fatigue for a C45 steel depending on stress ratio. Fatigue Fract. Eng. Mater. Struct. **44**, 2781–2799 (2021)
24. Fan, J., Guo, X., Zhao, X.: An energetic method to evaluate the macro and micro high-cycle fatigue behavior of the aluminum alloy. Proc. Inst. Mech. Eng. Part C J. Mech. Eng. Sci. **232**, 1456–1469 (2018)
25. Guo, Q., Guo, X., Fan, J., Syed, R., Wu, C.: An energy method for rapid evaluation of high-cycle fatigue parameters based on intrinsic dissipation. Int. J. Fatigue. **80**, 136–144 (2015)
26. Wang, X., Crupi, V., Jiang, C., Feng, E., Guglielmino, E., Wang, C.S.: Energy-based approach for fatigue life prediction of pure copper. Int. J. Fatigue. **104**, 243–250 (2017)
27. Guo, Q., Zaïri, F., Yang, W.: Evaluation of intrinsic dissipation based on self-heating effect in high-cycle metal fatigue. Int. J. Fatigue. **139**, 105653 (2020)
28. Mehdizadeh, M., Khonsari, M.M.: On the role of internal friction in low-and high-cycle fatigue. Int. J. Fatigue. **114**, 159–166 (2018)
29. Guo, Q., Guo, X.: Research on high-cycle fatigue behavior of FV520B stainless steel based on intrinsic dissipation. Mater. Des. **90**, 248–255 (2016)
30. Zhao, A., Xie, J., Zhao, Y., Liu, C., Zhu, J., Qian, G., Wang, S., Hong, Y.: Fatigue limit evaluation via infrared thermography for a high strength steel with two strength levels. Eng. Fract. Mech. **268**, 108460 (2022)
31. Colombo, C., Sansone, M., Patriarca, L., Vergani, L.: Rapid estimation of fatigue limit for C45 steel by thermography and digital image correlation. J. Strain Anal. Eng. Des. **56**, 478–491 (2021)
32. Meneghetti, G.: Analysis of the fatigue strength of a stainless steel based on the energy dissipation. Int. J. Fatigue. **29**, 81–94 (2007)
33. Shiozawa, D., Inagawa, T., Washio, T., Sakagami, T.: Fatigue limit estimation of stainless steels with new dissipated energy data analysis. Proc. Struct. Integr. **2**, 2091–2096 (2016)
34. Krapez, J.-C., Pacou, D., Bertin, C.: Application of lock-in thermography to rapid evaluation of fatigue limit in metals. In: Workshop on Advanced Infrared Technology and Applications (1999)
35. Krapez, J.-C., Pacou, D., Gardette, G.: Lock-in thermography and fatigue limit of metals. Quant. InfraRed Thermogr. (2000)
36. Jang, J., Khonsari, M.M.: On the evaluation of fracture fatigue entropy. Theor. Appl. Fract. Mech. **96**, 351–361 (2018)
37. Meneghetti, G., Ricotta, M.: Estimating the intrinsic dissipation using the second harmonic of the temperature signal in tension-compression fatigue: Part I. Theory. Fatigue Fract. Eng. Mater. Struct. **44**, 2168–2185 (2021)